International Journal of Science and Research (IJSR)
ISSN: 2319-7064
SJIF (2022): 7.942

Unlocking Prussian Blue Analogues: Enhancing Multimetallic Composition in Layered Double Hydroxides for Next-Gen Electrochemical Water Splitting

Manoj Kumar[1], Raghvendra Pratap Singh[2]

[1]Department of Chemistry, Kamla Nehru Institute of Physical and Social Sciences, Sultanpur, UP-228118, India
Email: *manojkumar35036[at]gmail.com*

[2]Department of Chemistry, Kamla Nehru Institute of Physical and Social Sciences, Sultanpur, UP-228118, India
Email: *rpsinghkni[at]gmail.com*

Abstract: ***The electrochemical water splitting is as a beacon of hope for future oxygen demands and sustainable energy solution. The oxygen evolution reaction (OER) experiences a sluggish kinetics due to simultaneous four-electron proton transfer reaction. The efficiency of this process hinges significantly the material used in reaction. Thus, the efficiency of electrochemical water splitting hindered and requires high potential. Herein In this regard, a series of electrocatalysts have been explored for electrochemical OER with high catalytic activity and stability. Herein, we have explored the high entropy Prussian blue analogue (HEPBA = MnFeCoNiCu-PBA) by simple solvothermal method for the electrochemical OER in alkaline medium. The multi-metallic composition, enhanced synergistic effect, and modulated structural and electronic properties provide the excellent OER activity, faster reaction kinetics, and stability. As a result, HEPBA showed the impressive OER activity at 260 mV overpotential to afford 10 mA cm^{-2} current density, lower than that of synthesized tetra-metallic (4-PBA), trimetallic (3-PBA), and bimetallic (2-PBA) analogue. Moreover, the high electrochemical surface area, lower charge transfer resistance and enhanced stability for 24 h have also recorded for HEPBA. Further, the electrochemical reconstruction of HEPBA has been established by spectroscopy and microscopy to form the active layered metal hydroxide-(oxy)hydroxide catalyst under anodic potential.***

Keywords: High entropy Prussian blue analogue; electrochemical reconstruction; ultrathin LDH nanosheets; synergistic effect; oxygen evolution

Highlights

- Facile synthesis of high entropy Prussian blue analogue precursor by solvothermal method.
- High synergistic effect of metals modulates the electronic structure.
- Electrochemical reconstruction into metal-(oxy)hydroxide active catalyst.
- Excellent oxygen evolution activity by high entropy Prussian blue analogue.

1. Introduction to Water Splitting and Its Importance

As the world grapples with the pressing challenges of climate change and the depletion of fossil fuels, the need for clean, renewable energy sources has never been more urgent. The electrochemical water splitting has attained great interest in the past few years due to the increasing demand of energy [1]. The oxygen evolution reaction (OER) is an anodic half-cell reaction of water splitting producing O_2 [2]. As the OER is accompanied by the simultaneous four electron and proton transfer process, the OER requires thermodynamic potential of 1.23 V *vs* RHE [3]. However, the electrocatalysts developed for the electrochemical OER require an extra potential (overpotential) to carry forward the overall reaction [3]. From the past few years, the precious metal (Ru/Ir) based electrocatalysts have been employed for the electrochemical OER in alkaline medium [4]. However, the rare abundance and high cost of the noble metals hamper their commercial application for large scale. In this regard, cost-effective earth abundant transition metal (Fe, Co, Ni, Mn) based materials such as metal oxides, hydroxides, phosphides, sulphides, selenides and nitrides have been explored with outstanding performance for the electrochemical OER [5,6].

Recently, a number of high entropy materials have been widely explored with the excellent catalytic performance and stability for electrochemical OER [7–10]. The high entropy materials are composed of five or more elemental components, where the concentration of the metal ions can be varied [11]. A series of high entropy materials like oxides, phosphides, sulphides, selenides and alloys have been demonstrated with enhanced OER activity and stability [7,12–14]. The enhanced OER activity of the high entropy materials is observed due to the (i) existence of high entropy, (ii) lattice distortion in the catalyst structure, (iii) good electronic conductivity, (iv) large number of accessible and exposed active sites, (v) improved synergistic effect and (vi) multi-metallic composition [15–18]. These unique properties provide the optimum binding energy for the adsorption of reaction intermediates promoting the OER activity [19].

For example, the high entropy $Fe_5Co_4Ni_{20}Se_{36}B_x$ catalyst was synthesized for electrochemical OER. The catalyst exhibited excellent OER performance at the requirement of 279.8 mV overpotential to deliver 10 mA cm^{-2} current density [20]. Due to the high synergistic effect, multi-metallic composition and increased active site, the charge transfer and water adsorption properties of the catalyst were enhanced facilitating the OER

activity [21–25]. Similarly, high entropy (CrMnFeCoNi)S_x was also developed for excellent electrochemical OER activity. The catalyst showed an overpotential of 295 mV to reach 100 mA cm^{-2} in alkaline medium [7]. The high electronic conductivity and enhanced charge and mass transport promoted the OER activity.

Recently, Prussian blue analogues (PBAs- a subcategory of metal-organic framework) have been demonstrated for the various applications like electrochemical energy storage, energy conversion, gas sorption etc. [26–29]. The PBAs are composed different metal ions interconnected with –CN bridged forming cubic structure. The PBAs have several unique advantages like (i) easy and facile synthesis, (ii) tunable structure and 3D morphology, (iii) large surface area, (iv) tunable porosity and (v) modulated electronic properties [11]. Owing to their unique properties, PBAs shows excellent electrochemical performance [7,11,28,30]. Previously, a series of PBA like CoFe-PBA, NiFe-PBA, CoFe-PBA@CC, CoFeCo-PBA@CC have been employed for electrochemical OER in alkaline medium [2].

These studies have established that the direct utilization of the PBAs for OER has the advantage of their facile electrochemical reconstruction into active layered double hydroxide catalyst (layered metal hydroxide-(oxy)hydroxide) during electrochemical OER [31–33]. The PBAs have been reported to endure complete and bulk reconstruction to form active metal hydroxide-(oxy)hydroxide [$M(OH)_2$-M(O)OH] nanosheets driven by anodic potential [33–35]. The active M(O)OH nanosheets exhibit excellent structural and electronic properties-(i) the active M(O)OH nanosheets are of atomic level providing the large surface area and exposed active sites, (ii) the nanosheets have optimum inter-layer distance, which can be tuned to promote the water adsorption properties, (iii) under the applied anodic potential, leaching of metals occurs resulting in the structural defects in active catalyst with cationic vacancies, (iv) the active nanosheets have metal centres with 3+/4+ oxidation states, which promote the O-O bond formation, and (v) the compositional and electronic structure tuning also result in the optimization of binding energy for the reaction intermediates improving the OER activity [2,4,36–40].

Motivated by previous reports, herein, we have developed high entropy MnFeCoNiCu-PBA (HEPBA) by simple solvothermal method and employed for electrochemical OER. Still now, the HEPBAs have never been utilized directly for electrochemical OER in alkaline medium. To the best of our knowledge, only one report is available where Ma et al. reported the high entropy-PBA Na_x(FeMnNiCuCo)[$Fe(CN)_6$] for the excellent sodium ion storage property. In our study, we have explored HEPBA and their tetrametallic, trimetallic, and bimetallic PBA analogue for the electrochemical OER. The study has shown that the increment in the entropy of the electrocatalyst by addition of the elements from bimetallic (MnFe-PBA) to high entropy PBA (MnFeCoNiCu-PBA) improves the OER activity due to the larger surface area, increased number of active sites and enhanced synergistic effects. Interestingly, HEPBA demonstrated remarkable OER activity at 260 mV overpotential to afford 10 mA cm^{-2} current density (figure 1). Moreover, the HEPBA furnished the outstanding OER activity for 24 h in alkaline medium.

2. The Role of Multimetallic Composition in Electrocatalysis

The role of multimetallic composition in electrocatalysis is pivotal, as it directly influences the efficiency and effectiveness of water splitting reactions[7,41]. In the quest for sustainable energy solutions, researchers have increasingly turned to layered double hydroxides (LDHs) as promising candidates for electrocatalysts. The essence of multimetallic systems lies in their ability to harness synergistic effects that enhance catalytic properties beyond those exhibited by their monometallic counterparts[42–44].

In these compositions, various metal ions are intercalated within the LDH structure, creating a unique environment that can significantly improve electrochemical performance. For instance, the introduction of metals like nickel, cobalt, or iron alongside traditional catalysts like ruthenium or platinum can lead to optimized charge transfer kinetics[43,45,46]. This is due to the modification of electronic properties that arise from the interactions between different metal species, which can lower activation energies and increase the surface area available for reaction.

Moreover, the tunability of multimetallic LDHs allows researchers to tailor the composition specifically for targeted applications. By adjusting the ratios of the constituent metals, one can enhance the selectivity and stability of the catalyst under operational conditions. This adaptability is crucial in the context of varying pH levels and temperatures encountered during electrochemical processes[47].

Notably, the incorporation of Prussian blue analogues within these multimetallic frameworks has opened new avenues for research and development. Their inherent electronic conductivity and high surface area complement the catalytic activity of the LDHs, ultimately leading to improved performance in water splitting applications. As we continue to explore the intricate dynamics of multimetallic interactions, the path toward more efficient and sustainable energy conversion technologies becomes clearer, promising a brighter future for oxygen and hydrogen production and beyond[2,48,49].

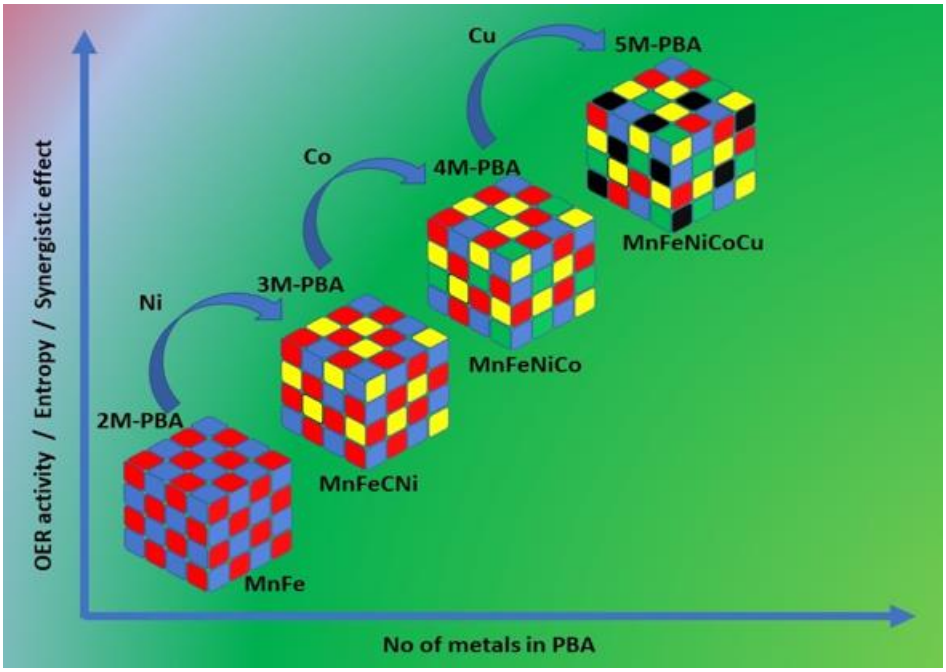

Figure 1: Schematic illustration for the synthesis of HEPBA by increasing the entropy of material through addition of metal ions. Color code: red-Mn, blue-Fe, green-Co, yellow-Ni and black-Cu. The OER activity of the catalyst is increased with increasing the entropy of the material & synergistic effect by successive addition of metal ions.

3. Result and discussion

3.1 Understanding High Entropy PBA

Composition and Properties Structural and morphological Characterization of HEPBA. The HEPBA was synthesized by solvothermal method using the different metal salts and $K_3[Fe(CN)_6]$ (see later in experimental section). Further, the HEPBA powder material was deposited on carbon cloth (CC) and characterized by using powder X-ray diffraction (PXRD). The PXRD pattern of HEPBA demonstrated the peaks, which were indexed for the cubic crystal structure of PBA having space group *Fm3m* (a=b=c and α=β=γ=90º). The PXRD pattern was well matched with the standard reference data JCPDF-01-077-1161 [50,51]. Fourier transform infrared spectroscopy (FTIR) was also carried out to detect the formation of HEPBA. The FTIR spectra identified the peak at 2098 cm^{-1}-2170 cm^{-1}, which was attributed to the asymmetric stretching vibrations of bridged –CN group in HEPBA [52–54]. These results confirmed the formation of cyanobridged HEPBA with cubic crystal structure.

The X-ray photoelectron spectroscopy (XPS) was performed to demonstrate the electronic environment and valence states of the elements in HEPBA. First, the Mn 2p XPS spectrum displayed two peaks at binding energies of 640.50 eV and 652.01 eV observed for Mn $2p_{3/2}$ and Mn $2p_{1/2}$, respectively(Figure 2a). The peak at 640.31 eV was assigned to the Mn^{2+} species in HEPBA [11,55–57]. The two peaks of Fe 2p XP-spectrum were originated at binding energies of 708.36 eV and 721.13 eV, ascribed to the Fe $2p_{3/2}$ and Fe $2p_{1/2}$, respectively(Figure 2b) [55,56,58,59]. The Fe 2p XPS confirmed the existence of Fe^{2+}/Fe^{3+} species in HEPBA. The Co 2p of XPS of HEPBA was deconvoluted into two peaks at binding energies 780.27 eV and 796.10 eV, corroborated to the Co $2p_{3/2}$ and Co $2p_{1/2}$, respectively. The peak at binding energy 780.27 eV was related to the Co^{2+} species(Figure 2c) [60–62]. The spin-orbit coupling spacing was also estimated to be 15.83 eV demonstrating the presence of Co^{2+} as major species in HEPBA [60–62].

The Ni 2p XPS revealed two peaks at binding energies of 854.15 eV and 871.69 eV assigned to the Ni $2p_{3/2}$ and Ni $2p_{1/2}$ respectively. The peak appeared at 854.09 eV was attributed to the presence of divalent Ni^{2+} species(Figure 2d) [55,57][63,64]. The Cu 2p XP spectrum was fitted into two peaks at binding energies of 933.30 eV (Cu $2p_{3/2}$), 953.71 eV (Cu $2p_{1/2}$) (Figure 2e). The peak at 933.30 eV was corresponded to the presence of Cu^{2+} [65,66]. The three peaks at binding energies of 398.84 eV, and 397.79 eV were fitted in N 1s XP-spectrum(Figure 2f), which could be correlated to the C=N and C≡N, respectively [67–69]. The C 1s XP spectrum confirmed the three peaks at binding energies 284.97 and 284.53 eV, which were originated for the C=C and C≡N respectively (Figure 2g) [67,68,70]. The O 1s XPS detected the two prominent peaks at 533.12 eV and 530.31 eV, (Figure 2h) observed due to the structural and/or adsorbed water and surface hydroxyl group, respectively [67,70].

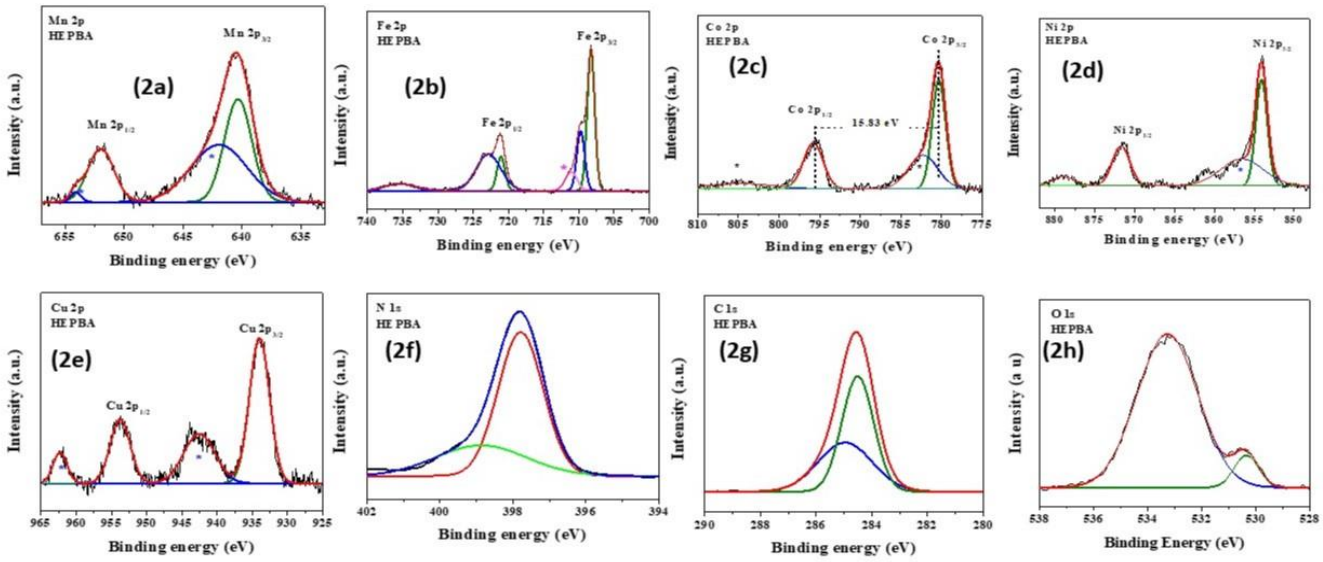

Figure 2: XPS of HEPBA of (2a) Mn 2p (2b) Fe 2p (2c) Co 2p (2d) Ni 2p (2e) Cu 2p (2f) N 1s (2g) C 1s (2h) O 1s.

3.2 Electrochemical activity of HEPBA

The synthesized PBAs were employed for electrochemical oxygen evolution reaction in aqueous 1.0 M KOH solution. The short cyclic voltammetry (CV) profile of HEPBA showed the pre-peak at 1.39 V vs RHE, which was attributed to the electrochemical oxidation of M^{2+} to M^{3+} under the applied anodic potential. It should be mentioned here that the pre-peak for the M^{2+}/M^{3+} oxidation was shifted anodically from 1.33 V vs RHE (4-PBA) to 1.39 V vs RHE (HEPBA).

The LSV profile showed that HEPBA furnished impressive OER activity at 260 mV overpotential to afford the current density 10 mA cm^{-2}, among the synthesized catalysts. In contrast, 4-PBA, 3-PBA, and 2-PBA produced the same current density but at higher overpotentials of 300 mV, 330 mV, and 450 mV, respectively (Figure 3a). It can be concluded here that increasing the entropy of PBA by addition of the metal ions drastically improved the OER activity. HEPBA expressed the outstanding OER activity than the noble metal-based RuO_2 catalysts. Moreover, HEPBA has been observed to possess better or comparable OER activity than the other PBA-derived catalysts and layered double hydroxides (LDHs).

The oxygen evolution kinetics of the studied catalyst were assessed from the Tafel plots. The lowest Tafel slope of 128 mV dec^{1} was recorded for HEPBA compared to other synthesized PBAs. The Tafel slopes of 4-PBA, 3-PBA, and 2-PBA were calculated to be 134 mV dec^{-1}, 161 mV dec^{-1}, 248 mV dec^{-1}, respectively (Figure 3b). The lowest Tafel slope of HEPBA revealed the faster oxygen evolution kinetics compared to the other catalysts. Further, the stability of HEPBA was evaluated under the chronoamperometric (CA) conditions. The CA plot displayed no significant decay in the current density indicating the excellent stability of HEPBA for 24 h. The increase in the current density for first few hours was attributed to the activation of HEPBA into active metal(oxy)hydroxide catalyst. After that, the current density was stabilized for the constant O_2 production.

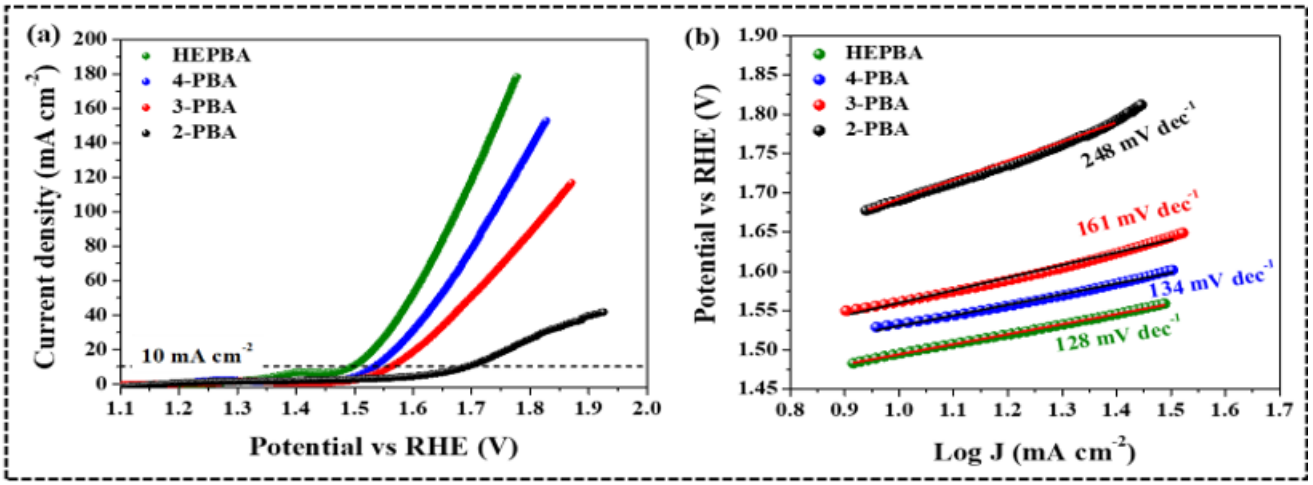

Figure 3: (a) LSV polarization curves for the oxygen evolution reaction of HEPBA compared with 4-PBA, 3-PBA, and 2-PBA showing the best OER activity of HEPBA and (b) Tafel plot for the oxygen evolution reaction of HEPBA compared with 4-PBA, 3-PBA, and 2-PBA showing the lowest Tafel slope value for HEPBA.

The enhanced catalytic performance of HEPBA could be attributed to the various electrochemical factors. First, the electrochemical impedance spectroscopy (EIS) was determined to evaluate the charge transfer properties of the synthesized PBAs. The lowest radius for the semicircle of HEPBA was evaluated in the EIS plot compared to other synthesized PBAs. This result clearly demonstrated the lowest charge transfer resistance (R_{ct}) of HEPBA among the synthesized catalysts. The lowest R_{ct} indicated the faster charge transfer properties of HEPBA, which resulted in the facile electron transfer improving the OER activity.

The double layer capacitance (C_{dl}) measurements were carried out to correlate the electrochemically active surface area (ECSA). The C_{dl} was calculated by the measurement of non-faradic capacitive current corresponding to the double layer charging. The ECSA of HEPBA was found to be 147.75 cm^2, largest among the synthesized catalysts. The largest ECSA value of HEPBA justified the presence of large number of electrochemically exposed active sites, which promoted the water adsorption properties to enhance the OER activity.

3.3 Structural and morphological Characterization after OER

Generally, transition metal-based catalysts are not real catalyst but they act as precatalyst and electrochemically reconstructed into $M(OH)_2$-$M(O)_x(OH)_y$ active catalyst driven by anodic potential during OER (Figure 4) [2,4,34,71,72]. The active $M(OH)_2$-$M(O)_x(OH)_y$ catalyst have ultrathin nature with atomic level thickness, more electrochemically active surface area and tuned structural and electronic properties.

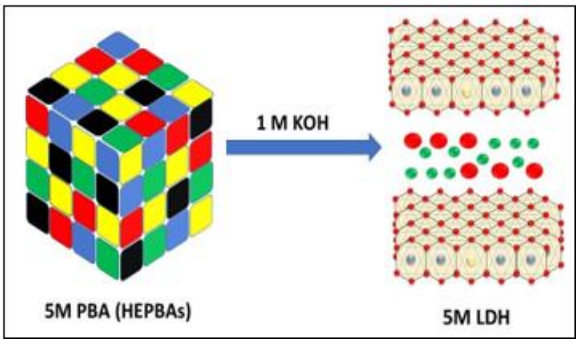

Figure 4: Schematic illustration for the electrochemical reconstruction of HEPBA into ultrathin layered hydroxide nanosheets.

The oxidation states and electronic environment of elements in the reconstructed active catalysts were evaluated using XPS studies. The XPS studies of Mn 2p, Fe 2p, Co 2p, Ni 2p and Cu 2p revealed the generation of the new peaks for high valent metal ions (M^{3+}) indicating the oxidation of metal centers under applied anodic potential [2,4,11,34,55–57]. The electrochemical reconstruction into active layered metal hydroxide-(oxy)hydroxide nanosheets under the applied anodic potential led to the generation of M^{3+} ions. The O 1s XPS spectrum was fitted in three peaks at 531.86 eV, 530.91 eV, and 529.52 eV, related to the adsorbed water molecules, surface –OH groups and metal-oxygen bond, respectively The origination of third peak for metal-oxygen bond confirmed the electrochemical reconstruction of HEPBA into active layered double hydroxide catalyst [4,34,71,73].

The spectroscopic and microscopic investigations confirmed the formation of ultrathin $M(OH)_2$-$M(O)_x(OH)_y$ nanosheets after 24 h OER-CA. The improved electrochemical performance of HEPBAs can be attributed to the following factors: i) the formation of ultrathin $M(OH)_2$-$M(O)_x(OH)_y$ nanosheets with tuned structural and electronic properties promoted the water adsorption and lower the free energy for reaction intermediates, ii) the presence of multi-metallic composition resulted in the enhanced synergistic effect increasing the charge transfer and mass transport properties, iii) high electrochemical surface area and increased number of active sites provided the faster water adsorption properties, and iv) presence of high valent metal ions M^{3+}/M^{4+} facilitated the formation of metal-oxo intermediates to improve the OER activity [2,4,34,71–73].

4. Conclusion

In conclusion, we have demonstrated high entropy Prussian blue analogue (HEPBA) by simple solvothermal method and utilized for electrochemical oxygen evolution. HEPBA reached a current density of 10 mA cm^{-2} at 260 mV overpotential, lower than that of synthesized catalysts. Moreover, the excellent stability of O_2 with HEPBA was also demonstrated for 24 h under chronoamperometric conditions. The introduction of different metal ions tuned the electronic structure and resulted in the enhanced synergistic effect, improved charge transfer properties, large number of active sites, high electrochemically active surface area and high electronic conductivity. Moreover, HEPBA was electrochemically reconstructed into active $M(OH)_2$-$M(O)_x(OH)_y$ nanosheets after 24 h OER-CA. The spectroscopic and microscopic studies have established the formation of HEPBA and their electrochemical reconstruction into active catalyst. The formation of ultrathin $M(OH)_2$-$M(O)_x(OH)_y$ nanosheets is considered as the key to promote the OER activity of HEPBA.

5. Experimental Section

5.1. Activation of carbon cloth

Firstly, the pieces of carbon cloth (CC) were prepared by cutting the CC into the small size of 2 cm x 1 cm. The pieces of carbon cloth were heated with concentrated HNO_3 at 100 ^oC for 4 hours. After natural cooling, the washing of the pieces of CC was performed with double distilled water followed by the drying in an air oven at 50 ^oC for 12 h.

5.2. Preparation of high entropy Prussian blue analogue (HEPBA)

A homogeneous solution (A) of metal salts of $Mn(CH_3COO)_2.4H_2O$ (0.375 mmol), $Co(CH_3COO)_2.4H_2O$ (0.375 mmol), $Ni(CH_3COO)_2.4H_2O$ (0.375 mmol), $Cu(CH_3COO)_2.H_2O$ (0.375 mmol) was prepared in 25 mL of distilled water. Further, a solution (B) was prepared by dissolving 1 mmol of $K_3[Fe(CN)_6]$ in 25 mL of distilled water. The solution B was mixed in solution A very slowly and stirred for 20 minutes for complete mixing. The mixture was aged at room temperature for 24 hours. After that, the mixture was centrifuged at the 10000 rpm for 10 minutes and followed

by washing with water and ethanol. Further, the obtained PBA (denoted as HEPBA) was dried at 60 ^{0}C for overnight.

5.3. Preparation of tetrametallic Prussian blue analogue (4-PBA)

The 4-PBA was also synthesized similar to the HEPBA. The 4-PBA was prepared by taking $Mn(CH_3COO)_2.4H_2O$ (0.5 mmol), $Co(CH_3COO)_2.4H_2O$ (0.5 mmol), $Ni(CH_3COO)_2.4H_2O$ (0.5 mmol) to form solution A.

For the comparison purpose, 3-PBA with the combination of MnFeCo ($Mn(CH_3COO)_2.4H_2O$ (0.75 mmol), $Co(CH_3COO)_2.4H_2O$ (0.75 mmol), and 2-PBA ($Mn(CH_3COO)_2.4H_2O$ (1.5 mmol) with combination of MnFe were also prepared by the similar procedure only keeping the mmol of metal salts to 1.5 mmol.

6. Electrochemical Measurements

The measurement of electrochemical performance of synthesized catalyst was carried out in a single three-electrode electrochemical cell in 1.0 M aqueous KOH solution. The 3 mg of HEPBA was dissolved in 50 µL of ethanol and 10 µL of 0.005 wt% Nafion solution was added to it followed by sonication of mixture for 30 minutes. The homogeneous suspension was drop-casted on 1 cm^2 surface area of carbon cloth. The deposited HEPBA@CC was utilized as working electrode and Pt wire was used in form of counter electrode. The Ag/AgCl was used as reference electrode. All the electrochemical experiments were performed in 1.0 M KOH solution (pH 13.8).

Cyclic voltammetry (CV) and linear sweep voltammetry (LSV) of synthesized PBAs were performed and expressed with 70% iR correction. All the potential measurements were converted into reversible hydrogen electrode (RHE) by using the formula:

$$E(RHE) = E(Ag/AgCl) + 0.197 + 0.059pH$$

The frequency range in electrochemical impedance spectroscopy (EIS) was from 0.001 to 100,000 Hz and amplitude of 10 mV. The calculations of charge transfers resistance (Rct) were performed from the diameter of the semicircle in the Nyquist plots. The experiment of chronoamperometric measurement (CA) was carried out in 1.0 M KOH solution at a particular constant potential and presented without iR compensation. The Tafel slope was determined at the potentials where current density was reached up to 10 mA cm^{-2}. The electrochemically active surface area (ECSAs) was evaluated by double layer capacitance (C_{dl}) measurement. The cyclic voltammetry (CV) for the C_{dl} measurement was performed at a potential range where apparent faradaic process not occurred. The ECSA of the synthesized catalyst was determined by the equation $ECSA=C_{dl}/C_s$ where C_s denotes the specific capacitance of the support for 1cm^2 of the real surface area.

Conflicts of interest

"There are no conflicts to declare."

Acknowledgments

Manoj Kumar acknowledges Central Research Facility (CRF) - IIT (Delhi) and IITR-Lab Lucknow for providing the characterization facilities.

Author Contribution

The synthesis of the catalysts, electrochemical experiments as well as data analysis was performed by Manoj Kumar. The manuscript was written by Manoj Kumar. The conceptualization, editing and reviewing were performed by Dr. R. P. Singh.

References

[1] J. Yao, W. Huang, W. Fang, M. Kuang, N. Jia, H. Ren, D. Liu, C. Lv, C. Liu, J. Xu, Q. Yan, Promoting Electrocatalytic Hydrogen Evolution Reaction and Oxygen Evolution Reaction by Fields: Effects of Electric Field, Magnetic Field, Strain, and Light, Small Methods. 4 (2020) 1–24. https://doi.org/10.1002/smtd.202000494.

[2] B. Singh, A. Yadav, A. Indra, Realizing electrochemical transformation of a metal-organic framework precatalyst into a metal hydroxide-oxy(hydroxide) active catalyst during alkaline water oxidation, J. Mater. Chem. A. 10 (2022) 3843–3868. https://doi.org/10.1039/d1ta09424f.

[3] F. Lyu, Q. Wang, S.M. Choi, Y. Yin, Noble-Metal-Free Electrocatalysts for Oxygen Evolution, Small. 15 (2019) 1–17. https://doi.org/10.1002/smll.201804201.

[4] B. Singh, O. Prakash, P. Maiti, A. Indra, Electrochemical Transformation of Metal Organic Framework into Ultrathin Metal Hydroxide-(oxy)hydroxide Nanosheets for Alkaline Water Oxidation, ACS Appl. Nano Mater. 3 (2020) 6693–6701. https://doi.org/10.1021/acsanm.0c01137.

[5] H. Xu, J. Wei, K. Zhang, M. Zhang, C. Liu, J. Guo, Y. Du, Constructing bundle-like Co-Mn oxides and Co-Mn selenides for efficient overall water splitting, J. Mater. Chem. A. 6 (2018) 22697–22704. https://doi.org/10.1039/c8ta07449f.

[6] P.W. Menezes, A. Indra, C. Das, C. Walter, C. Göbel, V. Gutkin, D. Schmeißer, M. Driess, Uncovering the Nature of Active Species of Nickel Phosphide Catalysts in High-Performance Electrochemical Overall Water Splitting, ACS Catal. 7 (2017) 103–109. https://doi.org/10.1021/acscatal.6b02666.

[7] M. Cui, C. Yang, B. Li, Q. Dong, M. Wu, S. Hwang, H. Xie, X. Wang, G. Wang, L. Hu, High-Entropy Metal Sulfide Nanoparticles Promise High-Performance Oxygen Evolution Reaction, Adv. Energy Mater. 11 (2021) 1–8. https://doi.org/10.1002/aenm.202002887.

[8] T.X. Nguyen, Y.H. Su, C.C. Lin, J.M. Ting, Self-Reconstruction of Sulfate-Containing High Entropy Sulfide for Exceptionally High-Performance Oxygen Evolution Reaction Electrocatalyst, Adv. Funct. Mater. 31 (2021) 1–11. https://doi.org/10.1002/adfm.202106229.

[9] B. Wang, Y. Yao, X. Yu, C. Wang, C. Wu, Z. Zou, Understanding the enhanced catalytic activity of high entropy alloys: From theory to experiment, J. Mater. Chem. A. 9 (2021) 19410–19438. https://doi.org/10.1039/d1ta02718b.

[10] R. Nandan, M.Y. Rekha, H.R. Devi, C. Srivastava, K.K. Nanda, High-entropy alloys for water oxidation: A new class of electrocatalysts to look out for, Chem. Commun. 57 (2021) 611–614. https://doi.org/10.1039/d0cc06485h.
[11] W. Jiang, T. Wang, H. Chen, X. Suo, J. Liang, W. Zhu, H. Li, S. Dai, Room temperature synthesis of high-entropy Prussian blue analogues, Nano Energy. 79 (2021) 105464. https://doi.org/10.1016/j.nanoen.2020.105464.
[12] J. You, R. Yao, W. Ji, Y. Zhao, Z. Wang, Research of high entropy alloys as electrocatalyst for oxygen evolution reaction, J. Alloys Compd. 908 (2022) 164669. https://doi.org/10.1016/j.jallcom.2022.164669.
[13] T. Wang, H. Chen, Z. Yang, J. Liang, S. Dai, T. Wang, H. Chen, Z. Yang, J. Liang, S. Dai, High-Entropy Perovskite Fluorides : A New Platform for Oxygen Evolution Catalysis High-Entropy Perovskite Fluorides : A New Platform for Oxygen Evolution Catalysis, (2020). https://doi.org/10.1021/jacs.9b12377.
[14] D. Lai, Q. Kang, F. Gao, High-entropy e ff ect of a metal phosphide on enhanced overall water splitting performance †, (2021) 17913–17922. https://doi.org/10.1039/d1ta04755h.
[15] Y. Ma, Y. Ma, Q. Wang, S. Schweidler, M. Botros, T. Fu, H. Hahn, T. Brezesinski, B. Breitung, High-entropy energy materials: Challenges and new opportunities, Energy Environ. Sci. 14 (2021) 2883–2905. https://doi.org/10.1039/d1ee00505g.
[16] Y. Qin, F. Wang, X. Wang, M. Wang, W. Zhang, W. An, X. Wang, Y. Ren, X. Zheng, D. Lv, A. Ahmad, Noble metal-based high-entropy alloys as advanced electrocatalysts for energy conversion, Rare Met. (2021). https://doi.org/10.1007/s12598-021-01727-y.
[17] J.K. Pedersen, T. Batchelor, A. Bagger, J. Rossmeisl, J.K. Pedersen, T.A.A. Batchelor, A. Bagger, High-Entropy Alloys as Catalysts for the CO 2 and CO Reduction Reactions, (2020).
[18] S.D. Lacey, Q. Dong, Z. Huang, J. Luo, H. Xie, Z. Lin, D.J. Kirsch, V. Vattipalli, C. Povinelli, W. Fan, R. Shahbazian-yassar, D. Wang, L. Hu, Stable Multimetallic Nanoparticles for Oxygen Electrocatalysis, (2019). https://doi.org/10.1021/acs.nanolett.9b01523.
[19] A.K. Singh, S. Ji, B. Singh, C. Das, H. Choi, P.W. Menezes, A. Indra, Alkaline oxygen evolution: exploring synergy between fcc and hcp cobalt nanoparticles entrapped in N-doped graphene, Mater. Today Chem. 23 (2022) 1–27. https://doi.org/10.1016/j.mtchem.2021.100668.
[20] Y. Zuo, D. Rao, S. Ma, T. Li, Y.H. Tsang, S. Kment, Y. Chai, Valence Engineering via Dual-Cation and Boron Doping in Pyrite Selenide for Highly Efficient Oxygen Evolution, ACS Nano. 13 (2019) 11469–11476. https://doi.org/10.1021/acsnano.9b04956.
[21] L. Zhang, W. Cai, N. Bao, Top-Level Design Strategy to Construct an Advanced High-Entropy Co–Cu–Fe–Mo (Oxy)Hydroxide Electrocatalyst for the Oxygen Evolution Reaction, Adv. Mater. 33 (2021) 1–10. https://doi.org/10.1002/adma.202100745.
[22] J. Park, H. Kim, S.Y. Kim, S.H. Ahn, Empirical approach for configuring high-entropy catalysts in alkaline water electrolysis, Int. J. Energy Res. 46 (2022) 9938–9947. https://doi.org/10.1002/er.7849.
[23] Adv Funct Materials - 2021 - Li - Multi-Sites Electrocatalysis in High-Entropy Alloys.pdf, (n.d.).
[24] P. Ma, S. Zhang, M. Zhang, J. Gu, L. Zhang, Y. Sun, W. Ji, Z. Fu, Hydroxylated high-entropy alloy as highly efficient catalyst for electrochemical oxygen evolution reaction, Sci. China Mater. 63 (2020) 2613–2619. https://doi.org/10.1007/s40843-020-1461-2.
[25] R. Wei, K. Zhang, P. Zhao, Y. An, C. Tang, C. Chen, X. Li, X. Ma, Y. Ma, X. Hao, Defect-rich FeCoNiPB/(FeCoNi)3O4-x high-entropy composite nanoparticles for oxygen evolution reaction: Impact of surface activation, Appl. Surf. Sci. 549 (2021) 149327. https://doi.org/10.1016/j.apsusc.2021.149327.
[26] A. Indra, U. Paik, T. Song, Boosting Electrochemical Water Oxidation with Metal Hydroxide Carbonate Templated Prussian Blue Analogues, Angew. Chemie - Int. Ed. 57 (2018) 1241–1245. https://doi.org/10.1002/anie.201710809.
[27] W. Ahn, M.G. Park, D.U. Lee, M.H. Seo, G. Jiang, Z.P. Cano, F.M. Hassan, Z. Chen, Hollow Multivoid Nanocuboids Derived from Ternary Ni–Co–Fe Prussian Blue Analog for Dual-Electrocatalysis of Oxygen and Hydrogen Evolution Reactions, Adv. Funct. Mater. 28 (2018) 1–11. https://doi.org/10.1002/adfm.201802129.
[28] Y. Ma, Y. Ma, S.L. Dreyer, Q. Wang, K. Wang, D. Goonetilleke, A. Omar, D. Mikhailova, H. Hahn, B. Breitung, T. Brezesinski, High-Entropy Metal–Organic Frameworks for Highly Reversible Sodium Storage, Adv. Mater. 33 (2021). https://doi.org/10.1002/adma.202101342.
[29] J.H. Lee, G. Ali, D.H. Kim, K.Y. Chung, Metal-Organic Framework Cathodes Based on a Vanadium Hexacyanoferrate Prussian Blue Analogue for High-Performance Aqueous Rechargeable Batteries, Adv. Energy Mater. 7 (2017). https://doi.org/10.1002/aenm.201601491.
[30] I. Hussain, C. Lamiel, M. Ahmad, Y. Chen, S. Shuang, M.S. Javed, Y. Yang, K. Zhang, High entropy alloys as electrode material for supercapacitors: A review, J. Energy Storage. 44 (2021) 103405. https://doi.org/10.1016/j.est.2021.103405.
[31] D. Zhao, Y. Lu, D. Ma, Effects of structure and constituent of prussian blue analogs on their application in oxygen evolution reaction, Molecules. 25 (2020). https://doi.org/10.3390/molecules25102304.
[32] A. Indra, A. Acharjya, P.W. Menezes, C. Merschjann, D. Hollmann, M. Schwarze, M. Aktas, A. Friedrich, S. Lochbrunner, A. Thomas, M. Driess, Boosting Visible-Light-Driven Photocatalytic Hydrogen Evolution with an Integrated Nickel Phosphide-Carbon Nitride System, Angew. Chemie. 129 (2017) 1675–1679. https://doi.org/10.1002/ange.201611605.
[33] X. Xu, H. Liang, F. Ming, Z. Qi, Y. Xie, Z. Wang, Prussian Blue Analogues Derived Penroseite (Ni,Co)Se2 Nanocages Anchored on 3D Graphene Aerogel for Efficient Water Splitting, ACS Catal. 7 (2017) 6394–6399. https://doi.org/10.1021/acscatal.7b02079.
[34] B. Singh, O. Prakash, P. Maiti, P.W. Menezes, A. Indra, Electrochemical transformation of Prussian blue analogues into ultrathin layered double hydroxide nanosheets for water splitting, Chem. Commun. 56

(2020) 15036–15039. https://doi.org/10.1039/d0cc06362b.
[35] L. Han, X.Y. Yu, X.W. (David) Lou, Formation of Prussian-Blue-Analog Nanocages via a Direct Etching Method and their Conversion into Ni–Co-Mixed Oxide for Enhanced Oxygen Evolution, Adv. Mater. 28 (2016) 4601–4605. https://doi.org/10.1002/adma.201506315.
[36] Z. Kou, X. Li, L. Zhang, W. Zang, X. Gao, J. Wang, Dynamic Surface Chemistry of Catalysts in Oxygen Evolution Reaction, Small Sci. 1 (2021) 2100011. https://doi.org/10.1002/smsc.202100011.
[37] J. Wang, S.J. Kim, J. Liu, Y. Gao, S. Choi, J. Han, H. Shin, S. Jo, J. Kim, F. Ciucci, H. Kim, Q. Li, W. Yang, X. Long, S. Yang, S.P. Cho, K.H. Chae, M.G. Kim, H. Kim, J. Lim, Redirecting dynamic surface restructuring of a layered transition metal oxide catalyst for superior water oxidation, Nat. Catal. 4 (2021) 212–222. https://doi.org/10.1038/s41929-021-00578-1.
[38] H. Jiang, Q. He, X. Li, X. Su, Y. Zhang, S. Chen, S. Zhang, G. Zhang, J. Jiang, Y. Luo, P.M. Ajayan, L. Song, Tracking Structural Self-Reconstruction and Identifying True Active Sites toward Cobalt Oxychloride Precatalyst of Oxygen Evolution Reaction, Adv. Mater. 31 (2019) 1–8. https://doi.org/10.1002/adma.201805127.
[39] H. Sun, Y. Zhu, W. Jung, J. Wang, X. Qian, H. Kong, molecules Tuning Reconstruction Level of Precatalysts to Design Advanced Oxygen Evolution Electrocatalysts, (2021). https://doi.org/10.3390/molecules26185476.
[40] A. Bergmann, E. Martinez-Moreno, D. Teschner, P. Chernev, M. Gliech, J.F. De Araújo, T. Reier, H. Dau, P. Strasser, Reversible amorphization and the catalytically active state of crystalline Co3O4 during oxygen evolution, Nat. Commun. 6 (2015). https://doi.org/10.1038/ncomms9625.
[41] J. Di, H. Zhu, J. Xia, J. Bao, P. Zhang, S.Z. Yang, H. Li, S. Dai, High-performance electrolytic oxygen evolution with a seamless armor core-shell FeCoNi oxynitride, Nanoscale. 11 (2019) 7239–7246. https://doi.org/10.1039/c8nr10191d.
[42] Y. Tian, S. Wang, E. Velasco, Y. Yang, L. Cao, L. Zhang, X. Li, Y. Lin, Q. Zhang, L. Chen, A Co-Doped Nanorod-like RuO2 Electrocatalyst with Abundant Oxygen Vacancies for Acidic Water Oxidation, IScience. 23 (2020) 100756. https://doi.org/10.1016/j.isci.2019.100756.
[43] X. Wang, R. Liu, Y. Zhang, L. Zeng, A. Liu, Hierarchical Ni 3 S 2 -NiOOH hetero-nanocomposite grown on nickel foam as a noble-metal-free electrocatalyst for hydrogen evolution reaction in alkaline electrolyte, Appl. Surf. Sci. 456 (2018) 164–173. https://doi.org/10.1016/j.apsusc.2018.06.107.
[44] J. Li, J. Song, B.Y. Huang, G. Liang, W. Liang, G. Huang, Y. Qi Jin, H. Zhang, F. Xie, J. Chen, N. Wang, Y. Jin, X.B. Li, H. Meng, Enhancing the oxygen evolution reaction performance of NiFeOOH electrocatalyst for Zn-air battery by N-doping, J. Catal. 389 (2020) 375–381. https://doi.org/10.1016/j.jcat.2020.06.022.
[45] J.W. Lang, L. Bin Kong, W.J. Wu, M. Liu, Y.C. Luo, L. Kang, A facile approach to the preparation of loose-packed Ni(OH) 2 nanoflake materials for electrochemical capacitors, J. Solid State Electrochem. 13 (2009) 333–340. https://doi.org/10.1007/s10008-008-0560-0.
[46] A. Higareda, D.L. Hernández-Arellano, L.C. Ordoñez, R. Barbosa, N. Alonso-Vante, Advanced Electrocatalysts for the Oxygen Evolution Reaction: From Single- to Multielement Materials, Catalysts. 13 (2023). https://doi.org/10.3390/catal13101346.
[47] Q. Jia, F. Su, Z. Li, X. Huang, L. He, M. Wang, Z. Zhang, S. Fang, N. Zhou, Tunable Hollow Bimetallic MnFe Prussian Blue Analogue as the Targeted pH-Responsive Delivery System for Anticancer Drugs, ACS Appl. Bio Mater. 2 (2019) 2143–2154. https://doi.org/10.1021/acsabm.9b00129.
[48] S. Chu, A. Majumdar, Opportunities and challenges for a sustainable energy future, Nature. 488 (2012) 294–303. https://doi.org/10.1038/nature11475.
[49] S. Venkata Mohan, A. Pandey, Sustainable Hydrogen Production, Biomass, Biofuels, Biochem. Biohydrogen, Second Ed. 305 (2019) 1–23. https://doi.org/10.1016/B978-0-444-64203-5.00001-0.
[50] H.J. Buser, A. Ludi, D. Schwarzenbach, W. Petter, The Crystal Structure of Prussian Blue: Fe4[Fe(CN)6]3·xH2O, Inorg. Chem. 16 (1977) 2704–2710. https://doi.org/10.1021/ic50177a008.
[51] J.F. Keggin, F.D. Miles, Structures and formulæ of the prussian blues and related compounds [4], Nature. 137 (1936) 577–578. https://doi.org/10.1038/137577a0.
[52] S.N. Ghosh, Infrared spectra of the Prussian blue analogs, J. Inorg. Nucl. Chem. 36 (1974) 2465–2466. https://doi.org/10.1016/0022-1902(74)80454-9.
[53] J. Lejeune, J.B. Brubach, P. Roy, A. Bleuzen, Application of the infrared spectroscopy to the structural study of Prussian blue analogues, Comptes Rendus Chim. 17 (2014) 534–540. https://doi.org/10.1016/j.crci.2014.01.017.
[54] H. Niwa, T. Moriya, T. Shibata, Y. Fukuzumi, Y. Moritomo, In situ IR spectroscopy during oxidation process of cobalt Prussian blue analogues, Sci. Rep. 11 (2021) 1–9. https://doi.org/10.1038/s41598-021-83699-8.
[55] X. Bie, K. Kubota, T. Hosaka, K. Chihara, S. Komaba, Synthesis and electrochemical properties of Na-rich Prussian blue analogues containing Mn, Fe, Co, and Fe for Na-ion batteries, J. Power Sources. 378 (2018) 322–330. https://doi.org/10.1016/j.jpowsour.2017.12.052.
[56] Y. Liu, D. He, R. Han, G. Wei, Y. Qiao, Nanostructured potassium and sodium ion incorporated Prussian blue frameworks as cathode materials for sodium-ion batteries, Chem. Commun. 53 (2017) 5569–5572. https://doi.org/10.1039/c7cc02303k.
[57] J. Li, L. He, J. Jiang, Z. Xu, M. Liu, X. Liu, H. Tong, Z. Liu, D. Qian, Facile syntheses of bimetallic Prussian blue analogues (KxM[Fe(CN)6]·nH2O, M=Ni, Co, and Mn) for electrochemical determination of toxic 2-nitrophenol, Electrochim. Acta. 353 (2020) 136579. https://doi.org/10.1016/j.electacta.2020.136579.
[58] Y. Huang, M. Xie, J. Zhang, Z. Wang, Y. Jiang, G. Xiao, S. Li, L. Li, F. Wu, R. Chen, A novel border-rich Prussian blue synthetized by inhibitor control as cathode for sodium ion batteries, Nano Energy. 39 (2017) 273–283. https://doi.org/10.1016/j.nanoen.2017.07.005.
[59] Y. Tang, W. Li, P. Feng, M. Zhou, K. Wang, Y. Wang, K. Zaghib, K. Jiang, High-Performance Manganese

Hexacyanoferrate with Cubic Structure as Superior Cathode Material for Sodium-Ion Batteries, Adv. Funct. Mater. 30 (2020). https://doi.org/10.1002/adfm.201908754.
[60] Y. Kang, S. Wang, K.S. Hui, H.F. Li, F. Liang, X.L. Wu, Q. Zhang, W. Zhou, L. Chen, F. Chen, K.N. Hui, [Fe(CN)6] vacancy-boosting oxygen evolution activity of Co-based Prussian blue analogues for hybrid sodium-air battery, Mater. Today Energy. 20 (2021) 100572. https://doi.org/10.1016/j.mtener.2020.100572.
[61] Y. Ma, Y. Ma, G. Giuli, T. Diemant, R.J. Behm, D. Geiger, U. Kaiser, U. Ulissi, S. Passerini, D. Bresser, Conversion/alloying lithium-ion anodes-enhancing the energy density by transition metal doping, Sustain. Energy Fuels. 2 (2018) 2601–2608. https://doi.org/10.1039/c8se00424b.
[62] A. Indra, P.W. Menezes, C. Das, C. Göbel, M. Tallarida, D. Schmeiβer, M. Driess, A facile corrosion approach to the synthesis of highly active CoOx water oxidation catalysts, J. Mater. Chem. A. 5 (2017) 5171–5177. https://doi.org/10.1039/c6ta10650a.
[63] Z. Wang, P. Guo, S. Cao, H. Chen, S. Zhou, H. Liu, H. Wang, J. Zhang, S. Liu, S. Wei, D. Sun, X. Lu, Contemporaneous inverse manipulation of the valence configuration to preferred Co2+ and Ni3+ for enhanced overall water electrocatalysis, Appl. Catal. B Environ. 284 (2021) 119725. https://doi.org/10.1016/j.apcatb.2020.119725.
[64] M. Khan, 美国科学院学报 Materials Chemistry A 材料化学 a, J. Mater. Chem. A. (2015) 121. https://doi.org/10.1039/C8TA12433G.Volume.
[65] Q. Wang, A. Sarkar, D. Wang, L. Velasco, R. Azmi, S.S. Bhattacharya, T. Bergfeldt, A. Düvel, P. Heitjans, T. Brezesinski, H. Hahn, B. Breitung, Multi-anionic and -cationic compounds: New high entropy materials for advanced Li-ion batteries, Energy Environ. Sci. 12 (2019) 2433–2442. https://doi.org/10.1039/c9ee00368a.
[66] X. Zhang, M. Xia, T. Liu, N. Peng, H. Yu, R. Zheng, L. Zhang, M. Shui, J. Shu, Copper hexacyanoferrate as ultra-high rate host for aqueous ammonium ion storage, Chem. Eng. J. 421 (2021) 127767. https://doi.org/10.1016/j.cej.2020.127767.
[67] J. Russat, Jean Russat, 11 (1988) 414–420.
[68] W.O. Silva, V. Costa Bassetto, D. Baster, M. Mensi, E. Oveisi, H.H. Girault, Oxidative Print Light Synthesis Thin Film Deposition of Prussian Blue, ACS Appl. Electron. Mater. 2 (2020) 927–935. https://doi.org/10.1021/acsaelm.9b00854.
[69] M. Kang, Z. Li, M. Hu, O. Oderinde, B. Hu, L. He, M. Wang, G. Fu, Z. Zhang, M. Du, Bimetallic MnCo oxide nanohybrids prepared from Prussian blue analogue for application as impedimetric aptasensor carrier to detect myoglobin, Chem. Eng. J. 395 (2020) 125117. https://doi.org/10.1016/j.cej.2020.125117.
[70] S. Wang, Z. Li, F. Duan, B. Hu, L. He, M. Wang, N. Zhou, Q. Jia, Z. Zhang, Bimetallic cerium/copper organic framework-derived cerium and copper oxides embedded by mesoporous carbon: Label-free aptasensor for ultrasensitive tobramycin detection, Anal. Chim. Acta. 1047 (2019) 150–162. https://doi.org/10.1016/j.aca.2018.09.064.
[71] B. Singh, A. Indra, Tuning the properties of CoFe-layered double hydroxide by vanadium substitution for improved water splitting activity, Dalt. Trans. 50 (2021) 2359–2363. https://doi.org/10.1039/d0dt04306k.
[72] B. Singh, A. Singh, A. Yadav, A. Indra, Modulating electronic structure of metal-organic framework derived catalysts for electrochemical water oxidation, Coord. Chem. Rev. 447 (2021) 214144. https://doi.org/10.1016/j.ccr.2021.214144.
[73] B. Singh, A.K. Patel, A. Indra, Introduction of high valent Mo6+ in Prussian blue analog derived Co-layered double hydroxide nanosheets for improved water splitting, Mater. Today Chem. 25 (2022) 100930. https://doi.org/10.1016/j.mtchem.2022.100930.